Computers and Geotechnics 91 (2017) 39–47

Contents lists available at ScienceDirect

Computers and Geotechnics

journal homepage: www.elsevier.com/locate/compgeo

Research Paper

Numerical study of slurry consolidometer tests taking into account the influence of wall friction

Wei He [a,b,*], David Williams [b], Ali Shokouhi [b]

[a] Changsha University of Science & Technology, Changsha, Hunan, China
[b] The University of Qeensland, Brisbane, QLD, Australia

ARTICLE INFO

Article history:
Received 10 January 2017
Received in revised form 6 June 2017
Accepted 21 June 2017

Keywords:
Slurried coal tailings
Slurry consolidometer
Sedimentation/consolidation theory
Wall friction
The finite element method

ABSTRACT

Three tests of slurried Jeeropilly coal tailings in a purpose-built slurry consolidometer under three different loading sequences were numerically analysed to study the friction losses quantitatively. A simplified sedimentation-consolidation theory was proposed to link the initial suspended state and soil-like state of slurries. The numerical simulations provided good agreement with the measured, and indicated the noticeable friction losses, from 11.1% to 34.2%, due to factors such as the diameter of consolidometers and loading sequences. The average coefficient of the stress (pore water pressure) stood at 1 at the beginning, and declined to a stable value around 0.55 (0.67).

1. Introduction

Slurries, such as dredging residues and mine tailings, undergo large settlement due to sedimentation and consolidation, which are required to be predicted [1–3]. This has prompted extensive experimental and theoretical studies of the problem over many decades [4–8].

Conventionally, the behaviour of slurries between the settling and the consolidation stage cannot be captured since they were studied in separate apparatus. These processes can be tested together in a slurry consolidometer which allows slurry to settle before consolidating under various loading sequences. However, comparing to conventional samples with maximum height-diameter ratio of approximately 2.5 [9], piston and wall friction in the slurry consolidometer is significant once the slurry develops effective stress, which complicates the interpretation and analysis of the results. Wickland & Wilson estimated in their large column tests that wall effects reduce vertical applied stresses by as much as 10–25% and could increase derived values of coefficient of volume change (m_v) and k by approximately 10–30%, based on a smooth-walled cell [10]. In order to determine the wall friction effects quantitatively, this paper considers the simulation of slurry consolidation test results using the finite element method.

2. Previous studies of sedimentation and consolidation

Conventional consolidometers such as the Rowe cells are usually of limited height (30 mm or 50 mm). However, to capture both the settling and consolidation behaviour, consolidometers need to accommodate relatively higher samples. A number of columns have been designed to study the settling and self-weight consolidation behaviour of a range of slurries, with no additional loading applied. Columns ranging in diameter from 47 to 1000 mm, and in height from 114 to 6000 mm, have been used [7,11–13,10]. There has been some further developments of columns, including accurately testing slurries of low densities and under low stresses [14]. Furthermore, the study of consolidation requires additional loadings on samples. Owen (1970) used a large consolidometer to study the consolidation of mud [15]. Bo et al. (1999) used a consolidometer measuring 495 mm in diameter and 1000 mm in height to study the deformation behaviour of slurry-like soil subjected to additional loading [16], whereas pore water in samples was drained radially due to the large diameter of the cell. Wong et al. (2008) conducted tests on fine-grained and non-segregation tailings in a consolidometer measuring 150 mm in diameter and 300 mm in height [17], but this consolidometer can only apply an additional load up to 20 kPa, which is insufficient for studying slurries consolidation behaviour. In order to overcome these problems, Shokouhi & Williams (2015) developed a slurry consolidometer measuring 150 mm in diameter and 410 mm in height, capable of applying

* Corresponding author at: Changsha University of Science & Technology, Changsha, Hunan, China.
E-mail address: wadeho@icloud.com (W. He).

http://dx.doi.org/10.1016/j.compgeo.2017.06.014
0266-352X/

a vertical stress of up to 500 kPa, to conduct tests on coal tailings slurry under a variety of loading sequences [18,19].

In slurry consolidometers, an aqueous slurry at an initial moisture content of well above its liquid limit is used to prepare a sample in suspension. This is of practical importance to understand the transition between the slurry state in which no particle-particle contact built, and the soil state in which particle-particle contact gives rise to effective stresses. Monte & Krizek tested a kaolinite clay slurry with an initial gravimetric moisture content of about 250% (approximately four or five times the liquid limit) and the void ratio at which effective stresses began was believed to be 7 [20]. Bo tested slurries with the void ratio in range of 2.1–2.68 [16,21]. De Oliveira-Filho and van Zyl [22]suggested that sedimentation of silt-sized soil ceases at a void ratio of 2.20, while Bartholomeeusen et al. suggested that the sedimentation of silt-sized river sediment ceases at void ratios between 2.09 and 4.48 [23]. Bonin et al. suggested a lower limiting void ratio than that suggested by both these authors [1]. Bo et al. suggested that the transition between a slurry and a soil can be determined from the void ratio at the peak pore pressure [24].

Apart from experimental studies, a number of techniques for the combined analysis of sedimentation and consolidation have been proposed. Been & Sills modified the linear solution of Gibson's equation in the light of observed experimental features to predict laboratory consolidation [7]. Pane & Schiffman linked pelagic sedimentation and consolidation as a single process governed by a modified effective stress equation, but detailed numerical solutions and laboratory verifications were not reported [8]. Toorman proposed semi-empirical relationships to form new closure equations of the unifying theory for sedimentation and self-weight consolidation [25]. Jeeravipoolvarn implemented a specific continuous interaction function to couple sedimentation and consolidation phenomena and examined the resulted model [3]. The represented effective stress-void ratio relationship in transition zone was further simplified in this paper. Bo proposed three compression indices for stresses covering three log cycles for ultra-soft soil to predict the magnitude and rate of settlement [26]. However, the influence of wall friction on parameters assessment is still unclear, which impedes these theories from reaching a better approximation of reality.

Some rough estimations on the influence of wall friction in slurry consolidometers were reported in the literature. Bo et al. estimated that friction on the side of the loading piston and on the wall reduced the stress applied to the slurry by 100–105 kPa on average [16]. Wong concluded that the effect of wall friction were difficult to quantify [17]. Umehara [27,11] and Shokouhi & Williams [18,19] reported on stress transducers mounted in the base plate and top cap to provide an estimate of the overall wall friction. Wickland et al. estimated wall friction in large-scale column tests on mixtures of mine waste rock and tailings to be 10–25% of the applied vertical stress [10]. In this paper, the finite element method has been used to study the influence of wall friction based on the results of large-strain consolidation tests under various loading sequences.

3. Wall friction in the purpose-built slurry consolidometer

As shown in Fig. 1, the slurry consolidometer was built by Wille-Geotechnik of Germany based on the specifications defined by The University of Queensland [18]. It consists of a stainless steel cell of 150 mm in internal diameter and 410 mm in height. The instrumentation includes: top and base load cells; 1000 kPa capacity pore water pressure transducers at mid-height, the base and halfway between the mid-height and base (i.e. at quarter-height); a 10 kN electromagnetic load frame; and a data logger and controller. The stress applied via a cap to the top of the specimen is measured by the top load cell connected to the loading piston, and the stress transmitted to the base is measured by the base load cell. The difference between the measured applied load at top and transmitted load to the base gives an indication of the combined piston and wall friction losses. The 410 mm height of the cell accommodates slurry samples to settle between layers, to make a test specimen with a hight of 300 mm high.

The stress distribution along specimens is difficult to measure, thus this distribution is commonly assumed in a linear or parabolic form [18,19], as shown in Fig. 2. It is intuitive that, the stress distribution is concave downward because of friction losses.

Generally, the average stress and pore water pressure of specimens can be calculated using,

$$\sigma_{ave} = \sigma_t - \beta_1(\sigma_t - \sigma_b) \tag{1}$$

and,

$$u_{ave} = \beta_2 u_b \tag{2}$$

where β_1 and β_2 are average coefficients. For linear and parabolic assumptions, $\beta_1 = \beta_2 = 0.5$ and $\beta_1 = \beta_2 = 0.67$, respectively.

As shown in Fig. 3, a slice of the specimen of infinitesimal thickness dz bounded by the walls of a large consolidometer may be considered. The vertical stress $\sigma(z)$ and $\sigma(z+dz)$ are applied respectively to the top and bottom of the slice, and the difference between them is the friction loss $f(z)$, which is proportional to the normal effective stress σ'_n developed on the wall. If the coefficient of proportionality is α, then the wall friction is given by,

$$\frac{d\sigma}{dz} = \alpha\sigma'_n \tag{3}$$

where $\alpha = tan\phi$ given by Coulomb's friction law, and ϕ is the wall friction angle.

The friction angle can be determined from direct shear box testing, with the material of the consolidometer wall filling the bottom half of the box and the soil filling the top half. For the purposes of this paper, the wall friction values recommended by NAVFAC were adopted [28]. Potyondy reported the results of a large number of direct shear box tests for various structural materials, and soil types at different pre-set water contents [29], which indicated much lower wall friction values than those recommended by NAVFAC.

The wall friction developed in a saturated soil may be given by Coulomb's friction law:

$$f = \sigma'_n \tan\phi \tag{4}$$

where ϕ is friction angle on the interface.

Including the radius of the large consolidometer r, the at rest lateral earth pressure coefficient against the wall K_0, and the wall friction angle ϕ, the coefficient of proportionality α is given by:

$$\alpha = \frac{2r\pi}{r^2\pi} K_0 \tan\phi \tag{5}$$

where K_0 is the lateral earth pressure coefficients at rest which can be estimated theoretically by Poisson's ratio.

4. Theory of large-strain consolidation

4.1. Large-strain formulations

Once a slurry settles to form particle-particle contact, the effective stresses develop under self-weight and any applied vertical stress. The strain accompanying the consolidation of settled slurries is too large to satisfy the assumptions of small strain, constant hydraulic conductivity, and constant compressibility. Gibson's general equation for large-strain consolidation is widely accepted [5], and can be expressed in volume fraction form as:

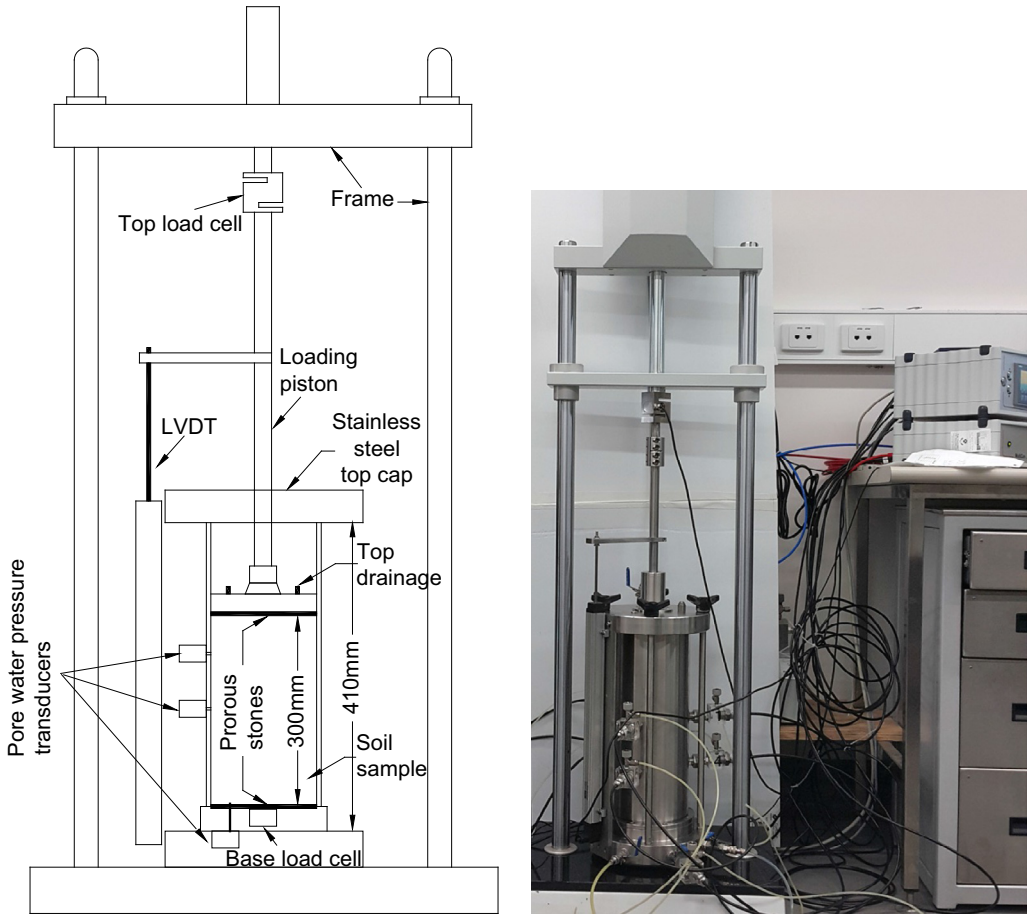

Fig. 1. Slurry consolidometer.

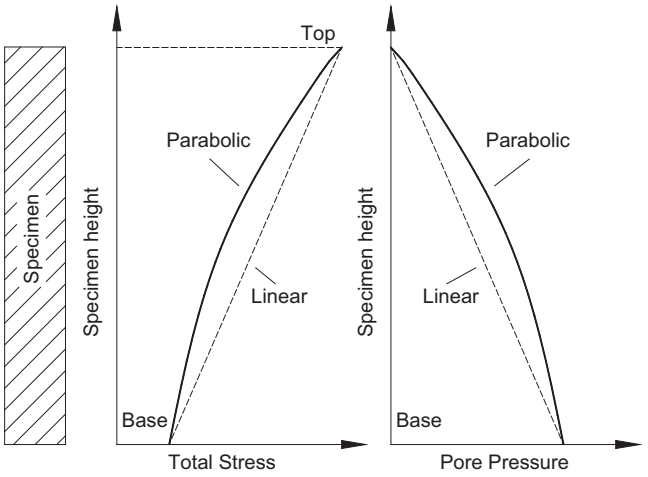

Fig. 2. Assumed stress distribution with specimen height.

$$\pm\left(\frac{\rho_s}{\rho_f}-1\right)\frac{d}{de}\left[\frac{k(e)}{1+e}\right]\frac{\partial e}{\partial \xi}+\frac{\partial}{\partial \xi}\left[\frac{k(e)}{\rho_f(1+e)}\frac{d\sigma'}{de}\frac{\partial e}{\partial \xi}\right]+\frac{\partial e}{\partial t}=0 \tag{6}$$

where ρ_s is the density of the solids, ρ_f is the density of the fluid, k is the hydraulic conductivity, e is the void ratio, ξ is the dimension in Lagrangian coordinates, σ'_n is the effective stress, and t is the time. ξ can be derived by,

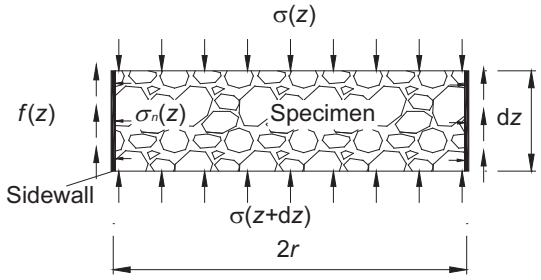

Fig. 3. Wall friction in a slurry consolidometer.

$$\frac{d\xi}{dz}=\frac{1}{1+e} \tag{7}$$

where z is dimension (depth) in Euler co-ordinates.

Koppla (1970) formulated the pore water pressure form of Eq. (6) as [30]:

$$\frac{d}{d\xi}\left(-\frac{k(e)}{\gamma_w(1+e)}\frac{du}{d\xi}\right)+\frac{de}{d\sigma'}\frac{\partial \sigma'}{\partial t}=0 \tag{8}$$

where γ_w is the unit weight of water. For self-weight consolidation [31], Eq. (8) can be transformed to:

$$\frac{d\sigma'}{dt}=(\gamma_s-\gamma_w)\frac{d(\Delta z)}{dt}-\frac{\partial u}{\partial t} \tag{9}$$

where γ_s is the unit weight of the solids, and δz is the consolidation settlement, and u is the pore water pressure. For consolidation

under the application of additional vertical stress, Eq. (9) can be transformed to:

$$\frac{d\sigma'}{dt} = \frac{d\Delta\sigma}{dt} - \frac{\partial u}{\partial t} \tag{10}$$

where $\Delta\sigma$ is the change in total stress. By rearranging Eq. (8), the governing equation becomes,

$$\frac{d}{d\xi}\left(-\frac{k(e)}{\gamma_w(1+e)}\right)\frac{du}{d\xi} - \frac{k(e)}{\gamma_w(1+e)}\frac{d^2u}{d\xi^2} + \frac{de}{d\sigma'}\left(\frac{\partial\sigma}{\partial t} - \frac{\partial u}{\partial t}\right) = 0 \tag{11}$$

In Lagrange co-ordinates, Eq. (3) becomes,

$$\frac{d\sigma}{d\xi} = \alpha\sigma'(1+e) \tag{12}$$

4.2. Initial suspension state

Large-strain consolidation theory is only able to capture the settlement behaviour of a soil once particle-particle contacts are formed, and effective stresses can develop. However, in the initial suspended state, there are no particle-particle contacts and no effective stresses can develop. Numerical analysis should incorporate the initial suspended state, although it may be unnecessary to couple sedimentation and large-strain consolidation.

Effective stress starts to develop at the maximum void ratio e_m, when consolidation occurs simultaneously with sedimentation til void ratio reaches the structural void ratio e_s. The zone between e_m and e_s is the so-called transition zone. Pane & Schiffman suggested a interaction coefficient β to consider this transition zone [8]. In this paper, The effective stress is simplified to increase linearly from zero at e_m to a certain value at e_s in semilog coordinate, as shown in Fig. 4.

In addition to the simplification of assuming a linear increase in effective stress with decreasing void ratio in the transition zone, a power function is usually suggested for the consolidation stage [32,3,31]. The complete mathematical formulation is,

$$e = \begin{cases} \frac{e_s - e_m}{\sigma^*}(\sigma' - \sigma^*) + e_s & e_s \leqslant e \leqslant e_m \\ A\sigma'^B & e \leqslant e_s \end{cases} \tag{13}$$

where σ^* is the effective stress at the transition between sedimentation and consolidation, and A and B are fitting parameters, generally obtained from laboratory test results.

To take into account wall friction effects in the large strain consolidation theory, Eq. (3) should be incorporated in the analysis. The commercially available software, FlexPDE 6.18, was implemented to solve the set of equations as a 1D problem. FlexPDE is a general-purpose software for obtaining numerical solutions to partial differential equations, based on the Finite Element Method.

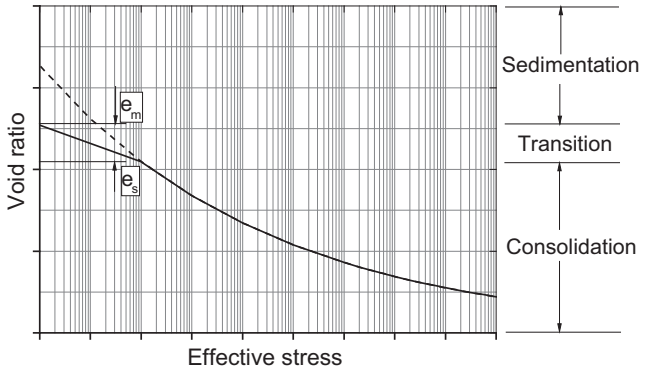

Fig. 4. Schematic of void ratio versus log_{10} effective stress sedimentation and consolidation [3].

For highly nonlinear problem such as the large strain consolidation, FlexPDE keeps oscillations to a minimum by refining mesh density and reducing time step in case that high error is detected. However, minor discontinuity of results is hardly avoided, as you may find in the analysis. In this analysis, two independent variables, namely total stress and pore water pressure, were solved based on the proposed equations. The limit of error in analyses was set to be 1×10^{-5} to keep oscillations to a minimum.

5. Numerical simulation of tests in the slurry consolidometer

5.1. Material and test methodology

The material tested was tailings collected from Jeebropilly Coal Mine, located in the Ipswich Coalfields of south-eastern Queensland, Australia. The tailings comprised about 83% sand-sized particles (0.06–2 mm), about 15% silt-sized particles (0.002–0.06 mm), and about 12% clay-sized particles (passing 0.002 mm) [33]. They were non-plastic, with a liquid limit of about 45%, and had a specific gravity of about 1.55. The tailings are classified as silty sand according to the Unified Soil Classification.

The Jeebropilly coal tailings are discharged at a solids concentration of about 25% by mass, and were prepared at this % solids for the large slurry consolidometer testing, using process make-up water. The average electrical conductivity and the pH of the process water were 3533 μs/cm and 8.7, respectively.

The test specimens were formed in three layers. The batch of slurry for each layer was prepared at a nominal solids concentration of 25% by mass (gravimetric moisture content of 300%, void ratio of about 5, dry density of about 0.25 t/m^3), and placed into the cell using a funnel and tube as a tremie. Some extra water was required to wash out the material remaining in the tube, resulting in a slight reduction of the solids concentration.

Each of the three layers was allowed to settle for about 2 h, and the supernatant water was removed and weighed prior to the next layer of slurry being placed. However after placing all layers, the specimens were allowed to settle more overnight.

The results of three tests, with each specimen subjected to different loading sequences, were numbered from T1 to T3 and numerically studied in this paper. As shown in Table 1: In Test T1, a constant rate of stress increase of 0.2 kPa/min was applied; in Test T2 the rate of stress increase was increased in a geometric series in seven increments; and in Test T3 the applied stress was

Table 1
Loading sequences applied.

Test no.	Loading step	Loading rate (kPa/min)	Duration of loading step (min)	Applied vertical stress (kPa)
T1	1	0.2	1500	300
	Total duration = 1500 min, Total applied vertical stress = 300 kPa			
T2	1	0.05	40	7
	2	0.1	40	16
	3	0.2	40	29
	4	0.4	40	50
	5	0.8	40	87
	6	1.6	40	156
	7	3.2	40	289
	Total duration = 2800 min, Total applied vertical stress = 289 kPa			
T3	1	0.2	250	50
	2	–	950	Held at 50
	3	–	1400	Held at 100
	4	–	1500	Held at 200
	5	–	3000	Held at 400
	Total duration = 7100 min, Maximum applied vertical stress = 400 kPa			

Table 2
Applied parameters in numerical models.

Test no.	Model no.	A (kPa^{-1})	B	C (m/s)	D	e_m
T1	N1	1.21	−0.07	4.5×10^{-8}	6	2
	N2	1.61	−0.07	1.5×10^{-8}	6	2
T2	N3	1.53	−0.11	2.7×10^{-7}	6	2
	N4	1.61	−0.08	3.0×10^{-8}	6	2
T3	N5	1.25	−0.08	2.0×10^{-8}	6	2
	N6	1.25	−0.08	3.0×10^{-7}	6	2
	N7	1.25	−0.06	3.0×10^{-7}	6	1.91

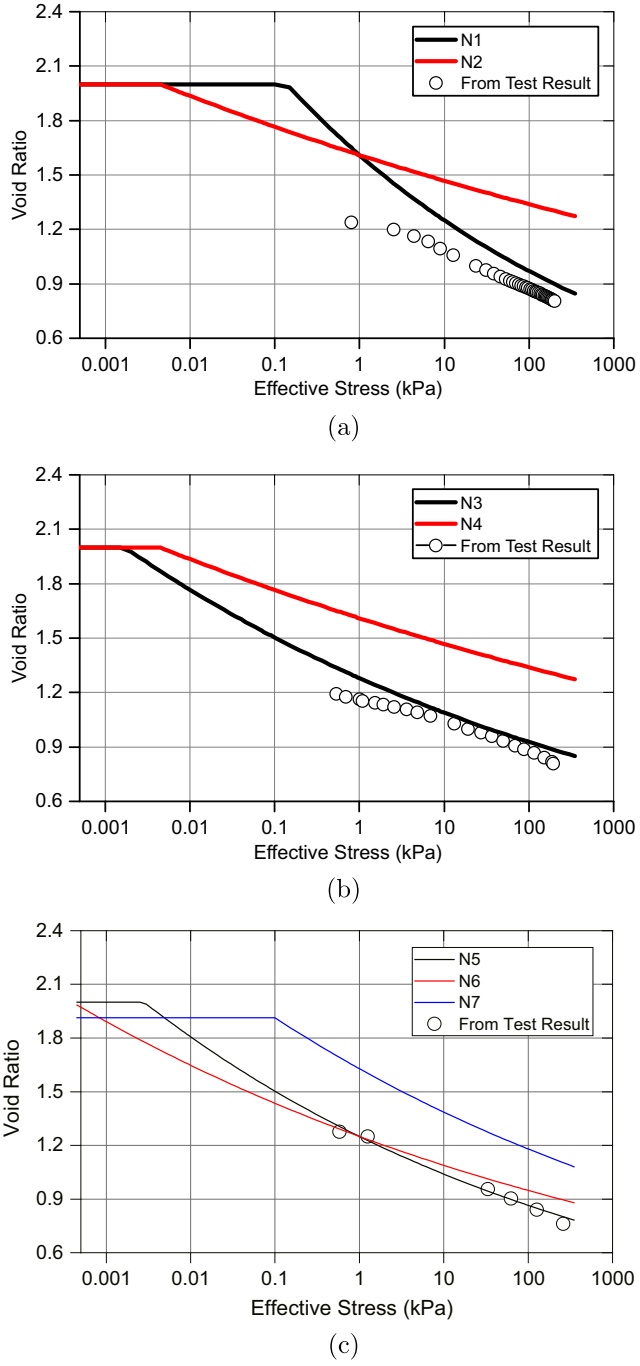

Fig. 5. Calculated void ratio versus $\log_{10}$ effective stress plots for each model: (a) T1; (b) T2; (c) T3.

doubled at each stage and held constant to the end of it. In each test, a seating stress of 5 kPa was first applied at a slow loading rate, controlled by pushing down the piston at the speed of 0.5 mm/min. Test data are recorded once the applied vertical stress reaches 5 kPa.

Each test specimen settled to a final solids concentration of about 50% by mass (gravimetric moisture content of about 100%, void ratio of 1.49–1.57, dry density of 0.60–0.62 t/m^3), to a height of 251–258 mm. The final consolidated solids concentration after loading was between 65% and 67% (gravimetric moisture content of between 49% and 52%, void ratio of between 0.76 and 0.81, dry density of between 0.86 t/m^3 and 0.88 t/m^3), with a final height of between 178 mm and 182 mm.

5.2. Parameters determination

The vital characteristics that have to be determined prior to numerical simulation include the maximum void ratio e_m, wall friction angle ϕ, and the relationships of $e - \sigma'$ and $e - k$.

To enable a numerical solution, it is necessary to start the slurry consolidation process at a void ratio of the order of 2, rather than at the experimental settled void ratio of 4.65. Since initial sedimentation and consolidation is very rapid, this assumption is reasonable, and is supported by the value of e_m selected by many authors [22,23].

Wall friction was modelled numerically using the test results of Potyondy [29], which gave a friction angle for saturated soil on steel, under low normal stress, of 24.5°.

To obtain $e - \sigma'$ relationships, effective stress was calculated by deducting measured pore water pressure from total stress, with the assumption of parabolic pressure profiles over the height of the slurry consolidometer specimens adopted [18,19]. The numerical parameters were then adjusted to obtain the best fit power relationships to the experimental $e - \sigma'$ curves.

In terms of $e - k$, Pane & Schiffman proposed a fluidization test to provide a direct conductivity measurement of clay suspensions, and suggested a two-constant power equation as [34],

$$k = Ce^D \tag{14}$$

where C and D are fitting parameters, which were determined by the trial-and-error approach in this paper.

A great amount of numerical analyses were carried out to obtain the best agreement with the experimental results, of which the seven results detailed in Table 2 and shown in Figs. 5 and 6 are reported herein. Fig. 5 also compared the average effective stress - void ratio relationship obtained from test results, to the parameters adopted in this paper.

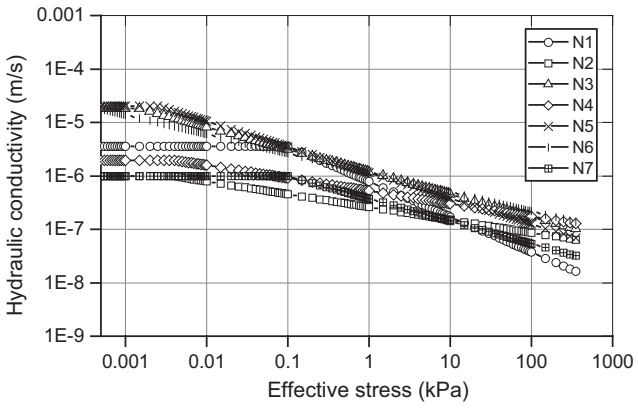

Fig. 6. $\log_{10}$ hydraulic conductivity versus $\log_{10}$ effective stress for each model.

5.3. Test results and numerical simulations

To compare the numerical results with the experimental results, the calculated stresses and pore water pressure at the base are compared with those obtained experimentally in Fig. 7. The origin of the plots in Fig. 7 was set at 167 min when the seating stress of 5 kPa had been reached. The numerical simulations are able to track the experimental results well, capturing the initial increase in pore water pressure and its rapid dissipation after a peak value is reached, and the loss of applied stress due to wall friction. Fig. 8 compares the calculated and measured settlements, which are not in quite as good agreement as the calculated stresses and pore water pressures, giving somewhat higher (conservative) calculated settlements.

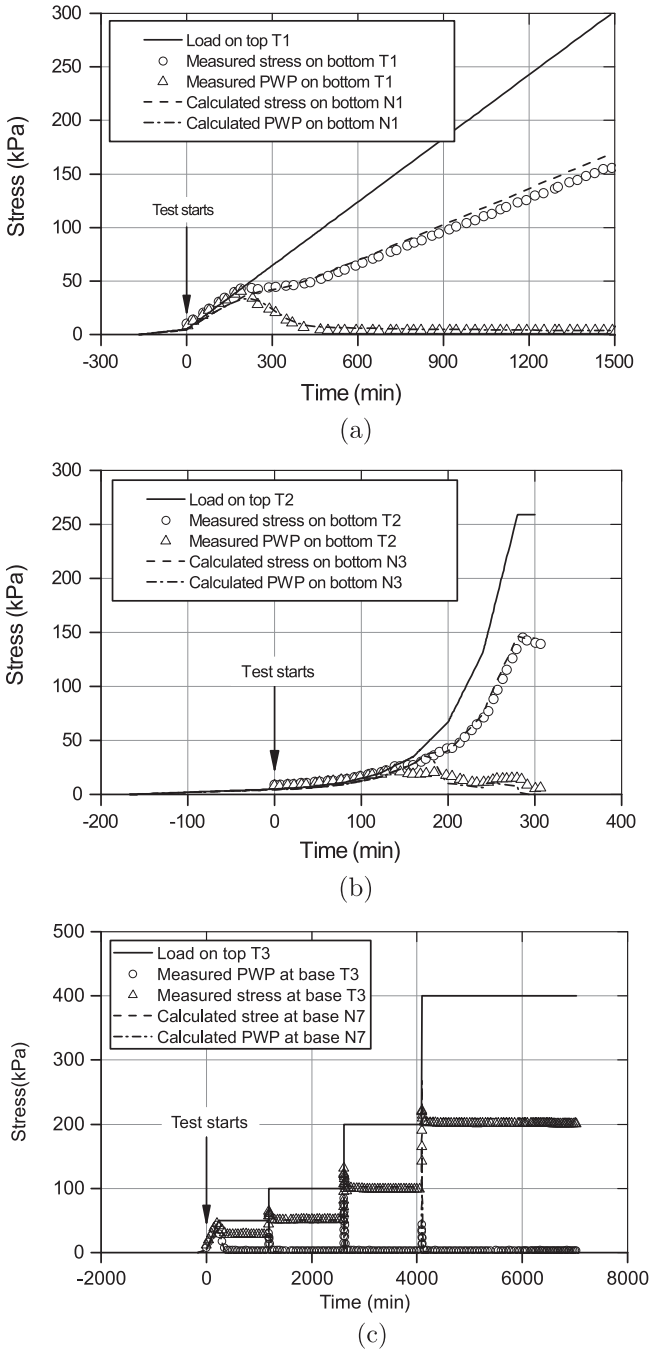

Fig. 7. Comparison of calculated and measured stresses for tests: (a) T1, (b) T2, (c) T3.

6. Discussions

6.1. Wall friction

The applied stress decreases with depth from the top of the specimen due to losses to wall friction, which has the same parabolic distribution as the effective stress according to Eq. (3). Typical distributions of total stress, pore water pressure and effective stress, calculated for Model No. N1 at 217 min after loading, are shown in Fig. 9. The total stress is a maximum where it is applied to the top piston, and decreases with depth due to accumulating wall friction. The pore water pressure drains rapidly at the only drainage boundary at the top of the specimen, and increases with depth, while the effective stress does the opposite. The increase in

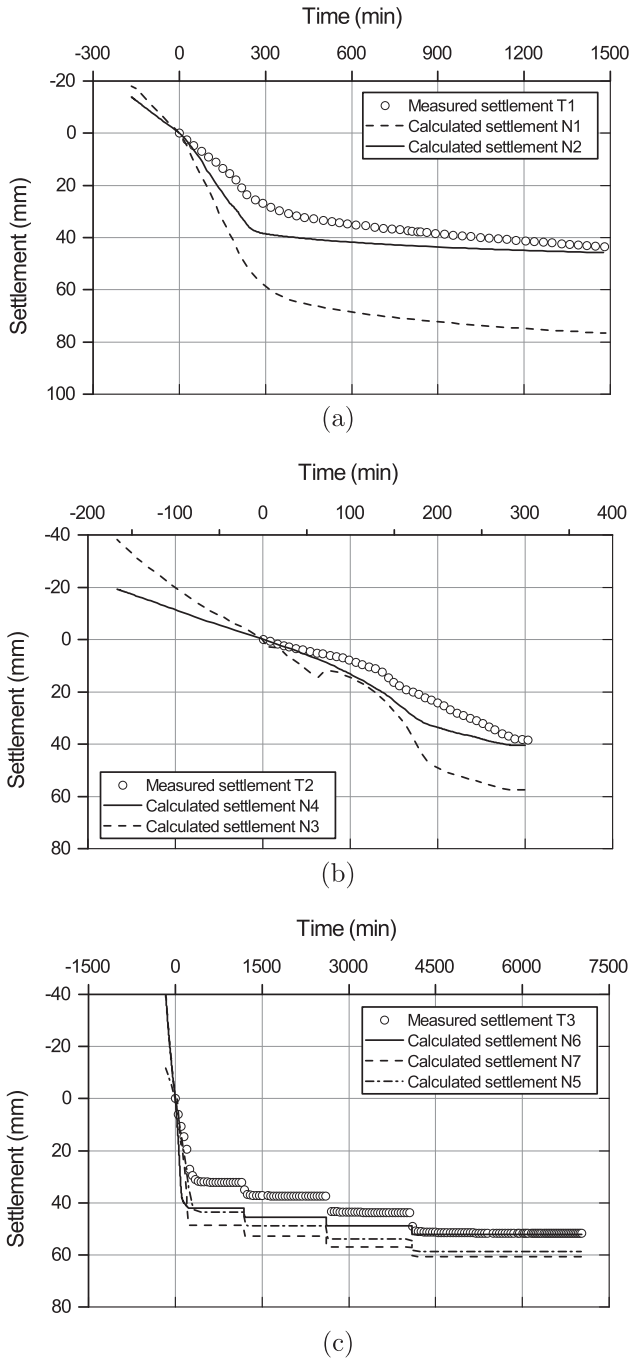

Fig. 8. Comparison of calculated and measured settlements for tests: (a) T1, (b) T2, (c) T3.

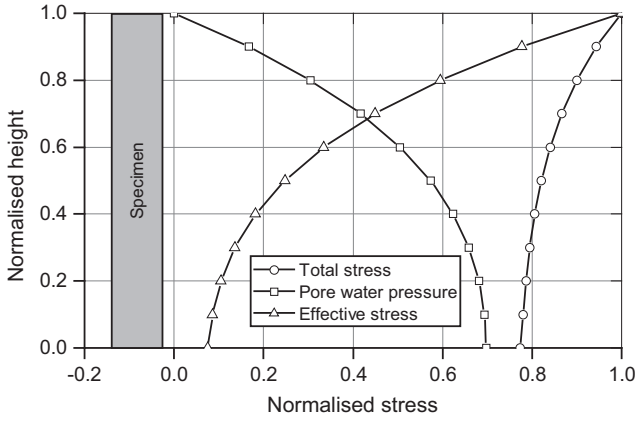

Fig. 9. Typical distribution of total stress, pore water pressure and effective stress.

wall friction with increasing total stress over time is shown in Fig. 10, which highlights the higher development of wall friction towards the top of the specimen, due to the higher effective stresses induced by top drainage.

Overall friction losses, which are shown in Fig. 11, were obtained by integrating total stresses for each test. The tests had similar friction losses (between 21% and 25%) at the end of loading, although higher loading rates slowed down the increase of overall friction losses in early stage. It is also indicated in the figure that, instantly applied vertical loads sharply reduce the friction losses in the model T3 under step-wise loading, and it went up promptly due to the quick dissipation of the excess pore water pressure.

Factors influencing wall friction include the diameter of the consolidometer, the lateral earth pressure coefficient at rest and, and the friction angle on the interface, of which the lateral earth pressure coefficient at rest and friction angle vary the least. The diameter of consolidometers described in the literature vary from 50 to 1000 mm. In order to determine the influence of consolidometer diameter on wall friction, four extra models were run based on Model No. N1, giving the total stress distributions shown in Fig. 12. The larger the diameter, the smaller is the wall friction or loss of stress at base. The effect of wall friction is seen in the reduction of the calculated base stress from 92% of the stress applied at the top for a 1000 mm diameter consolidometer to 17% for a 50 mm diameter consolidometer. For the 150 mm diameter slurry consolidometer results reported herein, the calculated base stress is 44% of the stress applied at the top.

Fig. 13 illustrates the maximum friction losses in the slurry consolidometer reported herein under different loading sequences, and the results were compared to that in consolidometers of

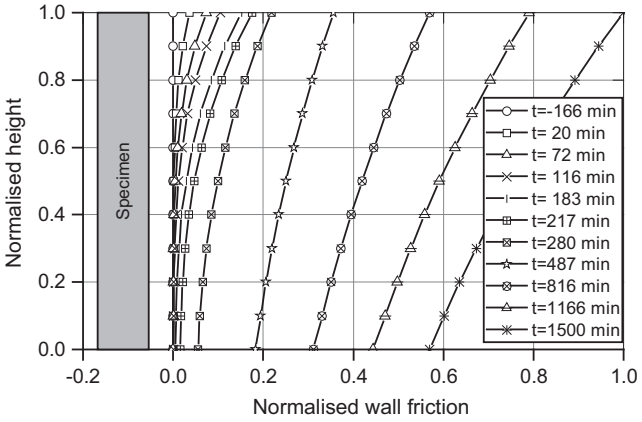

Fig. 10. Development of wall friction with increasing applied stress over time.

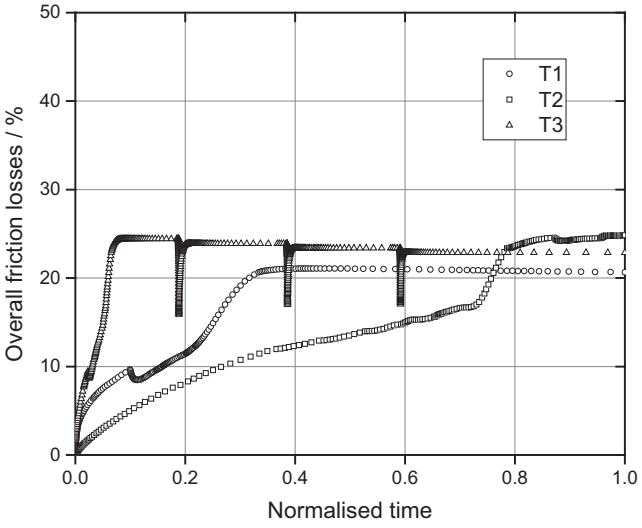

Fig. 11. Overall friction losses during each test.

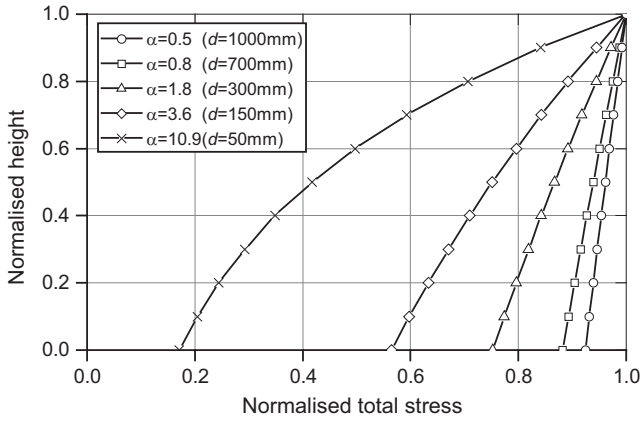

Fig. 12. Development of wall friction as a function of consolidometer diameter.

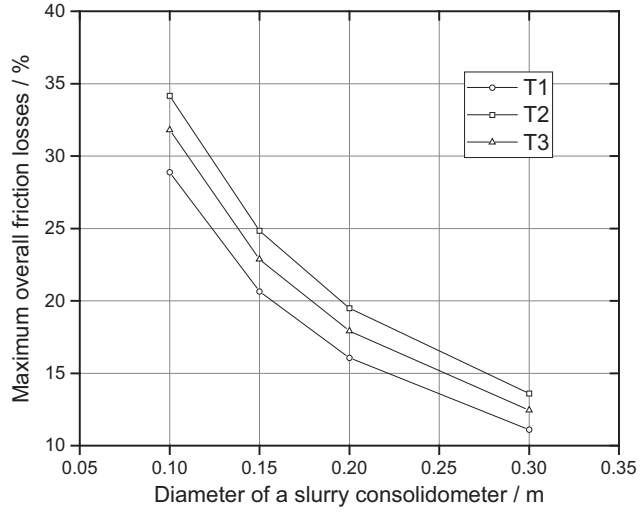

Fig. 13. Maximum overall friction losses versus the diameter of consolidometer.

0.1 m, 0.2 m, and 0.3 m in diameter. It is indicated that, the maximum overall friction losses decreased from 28.8–34.2% to 11.1–13.6%, with the increase in the diameter from 0.1 m to 0.3 m. The tests under the increasing rate of loading had the most considerable friction losses due to its highest loading rate.

6.2. Transition from a slurry to a soil

The initial increase in pore water pressure at the start of the slurry consolidometer tests and their subsequent rapid dissipation after reaching a peak value have been reported by many authors [24]. The development of pore water pressure represents the transition from a slurry to a soil-like state. The numerical analyses were extended to study this transition. Figs. 14 and 15 show, respectively, the calculated decreasing void ratio and decreasing hydraulic conductivity, with increasing applied stress over time. Simultaneously, the void ratio and hydraulic conductivity decrease from their initial maximum values, and the intersection between the developing void ratio and hydraulic conductivity represent the transition from a slurry to a soil. Below the transition point, effective stress is zero, and the pore water pressure will increase in reaction of the applied stress. The pore water pressure does not start to decrease until the transition point reaches the base of the specimen, when it dissipates at a rate dependent on the hydraulic conductivity.

6.3. Average coefficients for effective stress and pore water pressure

As shown in Fig. 16, the average coefficients, β_1 and β_2 in Eqs. (1) and (2), were back-analysed using the numerical results. In all tests, the average coefficients of effective stress and pore water pressure, namely β_1 and β_2, started from 1.0 (i.e. no friction losses at the very beginning). The values dropped to a stable value at around 0.55 and 0.67, respectively. The coefficient of pore water pressure, β_2, agreed with the parabolic assumption, while that of effective stress is slightly lower than it. Exclusively, in the Model T3, instant increase of loadings changed the average coefficient dramatically over a short period of time, then fell back again.

It is clear that, the variation rate of the average coefficients depends on loading rates, except for the characteristic of slurries. For example, the test No. 1 has the same loading rate, 0.2 kPa/min, as the test No. 3 in its first loading step, thus β_1 and

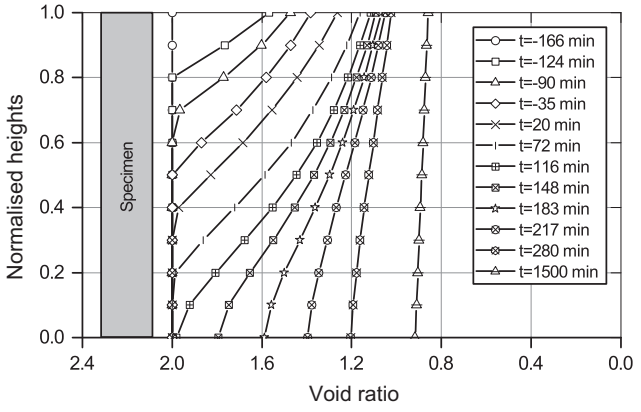

Fig. 14. Decreasing void ratio with increasing applied stress over time.

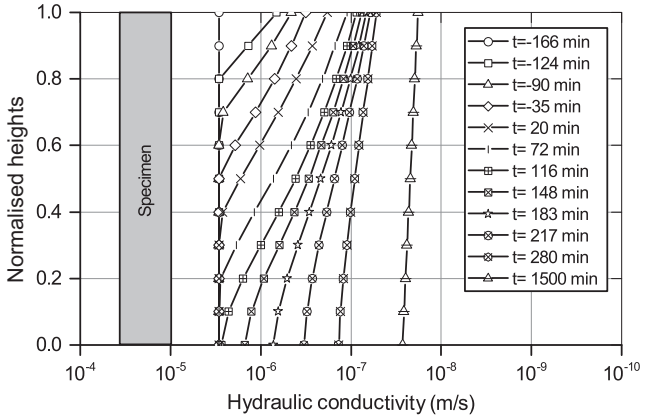

Fig. 15. Decreasing hydraulic conductivity with increasing applied stress over time.

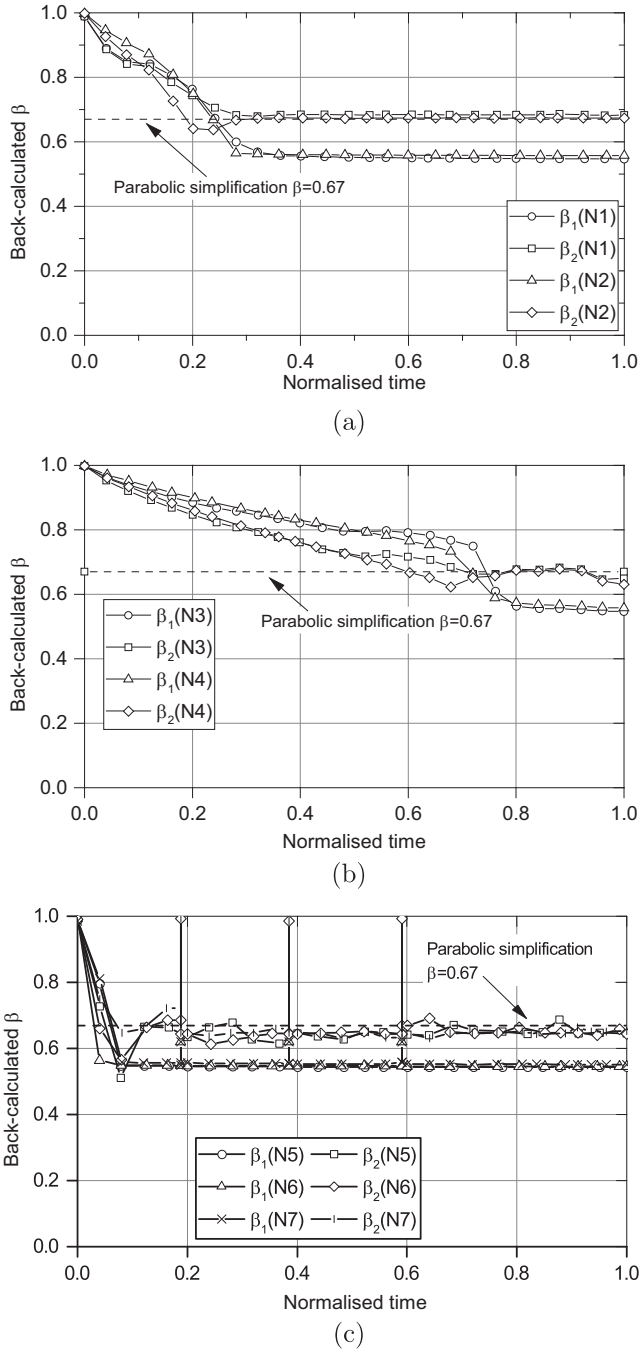

Fig. 16. Back calculated β_1 and β_2 for tests: (a) T1, (b) T2, (c) T3.

β_2 reached the stable value almost at the same time(just above 360 min). The higher the loading rate is, the longer time the average coefficients require to reach a stable value.

7. Conclusions

A numerical analysis was developed to study the influence of wall friction in a slurry consolidometer measuring 150 mm in diameter and 410 mm in height, based on the results of tests on slurried Jeeropilly coal tailings under different loading sequences. The paper reviews a range of laboratory large-strain consolidometers described in the literature, including the slurry consolidometer available at The University of Queensland. The theory of large-strain consolidation is also reviewed, including the modelling of the initial suspended state of the specimen, and the wall friction that develops in the consolidometer. The material characteristics, sample preparation, test apparatus, and the test results obtained for the coal tailing slurry tested in the slurry consolidometer are then described. In the three tests described, the loading sequences applied were: (i) a constant rate of loading, (ii) an increasing rate of loading, and (iii) step-wise loading.

The test results were modelled using the finite element method, including the necessary additional assumptions, the presentation of the numerical simulations, modelling the wall friction that develops, characterising numerically the transition from a slurry to a soil-like state, and calculating the average total stress and average pore water pressure during the tests.

The numerical models were able to simulate the slurry consolidometer test results well, providing good agreement with the measured stresses and pore water pressures for all loading cases, and reasonable agreement with measured settlements. Wall friction was well modelled, and the analyses allowed the decreasing hydraulic conductivity with increasing applied stress over time to be calculated. The intersection between the developing void ratio and hydraulic conductivity represent the transition from a slurry to a soil. Below the transition point, effective stress is zero, and the pore water pressure will increase in reaction of the applied stress. The pore water pressure does not start to decrease until the transition point reaches the base of the specimen, when it dissipates at a rate dependent on the hydraulic conductivity. For the consolidometer reported herein, considering that the diameter increase from 0.1 m to 0.3 m, the maximum overall friction losses decreased from 28.8–34.2% to 11.1–13.6%, under various loading sequences. The assumption of a parabolic distribution of total stress and pore water pressure with specimen depth was found to be reasonable after the pore water pressure had peaked in each test, with the average coefficient β_1 is 0.55 for effective stress and β_2 is 0.67 for pore water pressure. The time required for the average coefficients to reach the values depends on loading rates and characteristics of slurries.

Acknowledgements

The research on which this paper is based was supported by funding provided by the Australian Coal Association Research Program Project C19022 and the National Natural Science Foundation of China (No. 51478051). In addition, the authors wish to thank the management and staff of Jeebropilly Coal Mine, owned and operated by New Hope Corporation Australia, for providing tailings samples for testing.

References

[1] Bonin MD, Nuth M, Dagenais A-M, Cabral AR. Experimental study and numerical reproduction of self-weight consolidation behavior of thickened tailings. J Geotech Geoenviron Eng 2014;140(12):04014068.
[2] Rodríguez R, Sanchez M, Ledesma A, Lloret A. Experimental and numerical analysis of desiccation of a mining waste. Can Geotech J 2007;44(6):644–58.
[3] Jeeravipoolvarn S, Chalaturnyk R, Scott J. Sedimentation–consolidation modeling with an interaction coefficient. Comput Geotech 2009;36(5):751–61.
[4] Kynch GJ. A theory of sedimentation. Trans Faraday Soc 1952;48:166–76.
[5] Gibson R, England G, Hussey M. The theory of one-dimensional consolidation of saturated clays: 1. Finite non-linear consolidation of thin homogeneous layers. Geotechnique 1967;17(3):261–73.
[6] Michaels AS, Bolger JC. Settling rates and sediment volumes of flocculated kaolin suspensions. Ind Eng Chem Fundam 1962;1(1):24–33.
[7] Been K, Sills G. Self-weight consolidation of soft soils: an experimental and theoretical study. Geotechnique 1981;31(4):519–35.
[8] Pane V, Schiffman R. A note on sedimentation and consolidation. Geotechnique 1985;35(1):69–72.
[9] A. D2435/D2435M-11. Standard test methods for one-dimensional consolidation properties of soils using incremental loading. ASTM International, RFC ASTM D2435/D2435M-11. RFC Editor; 2011. URL <http://www.astm.org>.
[10] Wickland BE, Wilson GW, Wijewickreme D. Hydraulic conductivity and consolidation response of mixtures of mine waste rock and tailings. Can Geotech J 2010;47(4):472–85.
[11] Umehara Y, Zen K. Consolidation characteristics of dredged marine bottom sediments with high water content. Soils Found 1982;22(2):40–54.
[12] Alexis A, Bassoullet P, Le Hir P, Teisson C. Consolidation of soft marine soils: unifying theories, numerical modelling and in situ experiments. Coastal Eng Proc 1992;1(23):2949–61.
[13] Toorman EA, Berlamont JE. Mathematical modeling of cohesive sediment settling and consolidation. In: Nearshore and estuarine cohesive sediment transport; 1993. p. 167–84.
[14] Alexis A, Le Bras G, Thomas P. Experimental bench for study of settling-consolidation soil formation. ASTM Geotech Test J 2004;27(6):557–67.
[15] Owen M. Properties of a consolidating mud. Hydraulics Research Station; 1970.
[16] Win B, Choa V, Arulrajah A, Na Y. One-dimension compression of slurry with radial drainage. Soils Found 1999;39(4):9–17.
[17] Wong RCK, Mills BN, Liu YB. Mechanistic model for one-dimensional consolidation behavior of nonsegregating oil sands tailings. J Geotech Geoenviron Eng 2008;134(2):195–202. http://dx.doi.org/10.1061//ASCE/1090-0241/2008/134:2/195.
[18] Shokouhi A, Williams D. Volume change behaviour of mixtures of coarse coal reject and tailings. Min Technol. http://dx.doi.org/10.1080/14749009.2016.1277649.
[19] Shokouhi A, Williams D. One-dimensional settling and consolidation testing of dlurried coal tailings in a large slurry consolidometer, submitted to Engineering Geology Journal.
[20] Monte JL, Krizek R. One-dimensional mathematical model for large-strain consolidation. Geotechnique 1976;26(3):495–510.
[21] Bo MW, Chang MF, Arulrajah A, Choa V. Undrained shear strength of the Singapore marine clay at Changi from in-situ tests. Geotech Eng 2000;31(2):91–107.
[22] de Oliveira-Filho WL, van Zyl D. Modeling discharge of interstitial water from tailings following deposition. Part2: Application. Solos Rochas 2006;29(2):211–21.
[23] Bartholomeeusen G, Sills GC, Znidarc D, Kesteren WV, Merckelbach LM, Pyke R, Carrier WD, Lin H, Penumadu D, Winterwerp H, Masala S, Chan D. Sidere: numerical prediction of large-strain consolidation. Geotechique 2002;52(9):639–48.
[24] Win bo M, Choa V, Wong KS. Constant rate of loading test on ultra-soft soil. ASTM Geotech Test J 2010;33(3):192–200.
[25] Toorman E. Sedimentation and self-weight consolidation: constitutive equations and numerical modelling. Geotechnique 1999;49(6):709–26.
[26] Bo MW, Choa V, Wong KS, Arulrajah A. Laboratory validation of ultra-soft soil deformation model. Geotech Geol Eng 2011;29(1):65–74.
[27] Umehara Y, Zen K. Constant rate of strain consolidation for very soft clayey soils. Soil Found 1980;20(2):79–95.
[28] D.M. NAVFAC, 7.02, foundations & earth structures; 1986.
[29] Potyondy JG. Skin friction between various soils and construction materials. Geotechnique 1961;11(4):339–53.
[30] Koppula SD. The consolidation of soil in two dimensions and with moving boundaries. Phd thesis; 1970.
[31] Ito M, Azam S. Large-strain consolidation modeling of mine. Environ Syst Res 2013;2:1–12.
[32] Townsend F, McVay M. SOA: large strain consolidation predictions. J Geotech Eng 1990;116(2):222–43.
[33] Williams D. Chapter 17: placing covers on soft tailings. Ground improvement-case histories. Oxford; Elsevier: p. 491–512.
[34] Pane V, Schiffman R. The permeability of clay suspensions. Geotechnique 1997;47(2):273–88.